QUANTUM MAGNETISM

Resolving quanta of collective spin excitations in a millimeter-sized ferromagnet

Dany Lachance-Quirion,[1,2] Yutaka Tabuchi,[2] Seiichiro Ishino,[2] Atsushi Noguchi,[2] Toyofumi Ishikawa,[2] Rekishu Yamazaki,[2] Yasunobu Nakamura[2,3*]

Combining different physical systems in hybrid quantum circuits opens up novel possibilities for quantum technologies. In quantum magnonics, quanta of collective excitation modes in a ferromagnet, called magnons, interact coherently with qubits to access quantum phenomena of magnonics. We use this architecture to probe the quanta of collective spin excitations in a millimeter-sized ferromagnetic crystal. More specifically, we resolve magnon number states through spectroscopic measurements of a superconducting qubit with the hybrid system in the strong dispersive regime. This enables us to detect a change in the magnetic moment of the ferromagnet equivalent to a single spin flipped among more than 10^{19} spins. Our demonstration highlights the strength of hybrid quantum systems to provide powerful tools for quantum sensing and quantum information processing.

INTRODUCTION

Engineering interactions between photons and quanta of excitations in atomic and solid-state systems are central to the development of quantum technologies. Cavity and circuit quantum electrodynamics have enabled the realization of many gedanken experiments in quantum optics (*1*–*3*), as well as offering a promising platform for quantum computing (*4*–*7*). Ideas from these fields have been successfully transposed to other architectures such as optomechanical systems (*8*). In these systems, phonons in mechanical modes can interact with photons of both microwave and optical domains, offering a promising platform for transducing quantum information between microwave-only quantum systems, such as superconducting qubits, and photons in optical fibers (*8*–*10*).

Recently, a novel approach enabling bidirectional conversion between microwave and optical photons using their mutual interaction with macroscopic collective spin excitation modes in ferromagnetic insulators has been explored (*11*–*14*). Combined with the coherent interaction between the magnons in these magnetostatic modes and superconducting qubits (*15*, *16*), this demonstration opens up the possibility of transducing quantum information between a superconducting quantum processor and photons in optical fibers. However, a key ingredient for using quantum magnonics systems as quantum transducers is the capability of encoding arbitrary qubit states in magnon nonclassical states.

RESULTS

The coherent interaction between magnons and a superconducting qubit was previously demonstrated through the observation of a magnon-vacuum Rabi splitting of the qubit (*15*). Here, we go further and explore the off-resonant, dispersive regime of quantum magnonics, a promising regime to probe and control magnon states using the superconducting qubit. In circuit quantum electrodynamics, the strong dispersive interaction between a qubit and a microwave cavity has been used as a quantum sensor of the electromagnetic field of the cavity (*17*, *18*) and to create and manipulate nonclassical states of microwave light (*19*, *20*). Here, we demonstrate the ability to reach the strong dispersive regime in quantum magnonics by probing magnons at the level of single quanta in a millimeter-sized ferromagnet using spectroscopic measurements of the qubit. Our demonstration opens up the possibility of measuring, creating, and manipulating macroscopic nonclassical magnon states in ferromagnetic systems.

Our hybrid system consists of a superconducting qubit and a single-crystalline yttrium iron garnet (YIG) sphere inside a three-dimensional microwave cavity (Fig. 1A). The transmon-type superconducting qubit has a resonant frequency of 7.9905 GHz (*21*). A pair of permanent magnets and a coil are used to apply a magnetic field B_0 to the YIG sphere, making it a single-domain ferromagnet. The electric dipole of the qubit and the magnetic dipole of the ferromagnet couple to the electric and magnetic fields of the cavity modes, respectively. The YIG sphere is placed near the antinode of the magnetic field of the transverse electric TE_{102} cavity mode, so that the cavity field is nearly uniform throughout the 0.5-mm sphere. This makes the uniformly precessing mode, or Kittel mode, the most dominantly coupled magnetostatic mode. As detailed in section S2, the interaction strength $g_{m\text{-}c}$ between the TE_{102} cavity mode, or coupler mode, and the Kittel mode reaches the strong coupling regime (*22*–*26*), where $g_{m\text{-}c}/2\pi$ = 22.5 MHz is much larger than both the cavity ($\kappa_c/2\pi$ = 2.08 MHz) and magnon ($\gamma_m/2\pi$ = 1.3 MHz) linewidths.

The coupling of the superconducting qubit and the Kittel mode to the same cavity modes creates an effective interaction between these two macroscopic systems (*15*, *16*). To verify that this interaction is coherent, we perform spectroscopic measurements of the qubit with the hybrid system in the quantum regime at a temperature of 10 mK. Although the qubit-magnon coupling is mostly provided by the TE_{102} cavity mode at 8.4563 GHz (coupler mode), we use the dispersive interaction of the qubit with the TE_{103} cavity mode at 10.4492 GHz (probe mode) to read out the qubit. This scheme avoids measurement-induced dephasing caused by photon number fluctuations in the coupler mode (*16*, *17*). The change in the reflection coefficient r of a probe microwave tone, resonant with the probe mode and containing less than one photon on average, is measured while exciting the qubit with a spectroscopic microwave tone at frequency ω_s. Figure 1B shows the real part of the change of the reflection coefficient, Δr, measured for different currents I in the coil, changing the frequency $\omega_m \propto B_0$ of the magnons in the Kittel mode. The avoided crossing indicates the

[1]Institut quantique and Département de Physique, Université de Sherbrooke, Sherbrooke, Québec J1K 2R1, Canada. [2]Research Center for Advanced Science and Technology, University of Tokyo, Meguro-ku, Tokyo 153-8904, Japan. [3]Center for Emergent Matter Science, RIKEN, Wako, Saitama 351-0198, Japan.
*Corresponding author. Email: yasunobu@qc.rcast.u-tokyo.ac.jp

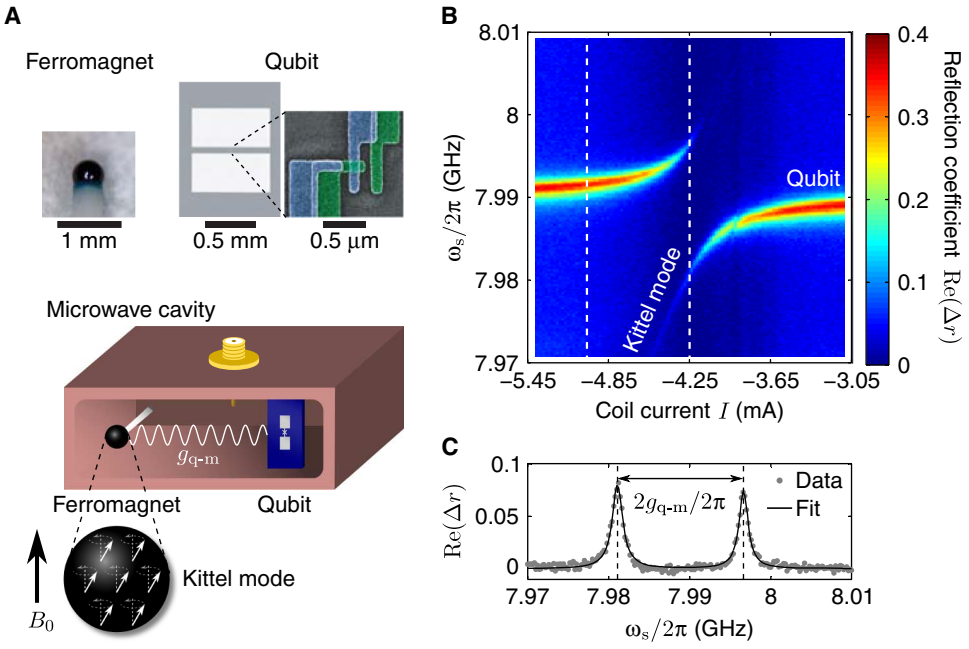

Fig. 1. Hybrid system and qubit-magnon coherent interaction. (**A**) Schematic illustration of a ferromagnetic YIG sphere and a superconducting transmon qubit inside a three-dimensional microwave cavity. A magnetic field B_0 is applied to the YIG sphere using permanent magnets and a coil. The magnetostatic mode in which spins uniformly precess in the ferromagnetic sphere, or the Kittel mode, couples to the magnetic field of the cavity modes. The qubit and the Kittel mode interact through virtual excitations in the cavity modes at a rate $g_{q\text{-}m}$. (**B**) The spectrum of the qubit is measured by probing the change of the reflection coefficient Re(Δr) of a microwave excitation resonant, with the probe mode at frequency ω_p as a function of the spectroscopy frequency ω_s and the coil current I, changing the magnetic field at the ferromagnet. The avoided crossing indicates a coherent interaction between the qubit and the Kittel mode. Vertical dashed lines indicate that I = −4.25 mA, where the qubit and the Kittel mode are hybridized (Fig. 1D), and that I = −5.02 mA, where the qubit-magnon interaction is in the dispersive regime (Figs. 2 to 4). (**C**) Magnon-vacuum Rabi splitting of the qubit on resonance, with the Kittel mode at I = −4.25 mA. From the fit, we extract the qubit-magnon coupling rate $g_{q\text{-}m}/2\pi$ = 7.79 MHz.

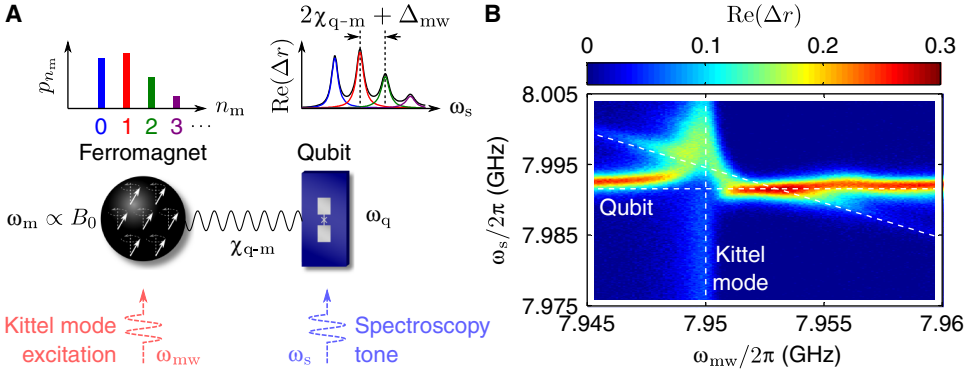

Fig. 2. Dispersive qubit-magnon interaction. (**A**) Schematic illustration of the hybrid system in the strong dispersive regime. A microwave excitation at frequency ω_{mw} is used to create a magnon coherent state in the Kittel mode. The excitation is detuned from the magnon frequency, with the qubit in the ground state, $\omega_m{}^g$, by $\Delta_{mw} = \omega_m{}^g - \omega_{mw}$. In the strong dispersive regime, magnon number states $|n_m\rangle$ (of probability distribution p_{n_m}) are mapped into the qubit spectrum as peaks at frequencies $\tilde{\omega}_q^{(n_m)} = \omega_q^{(n_m)} + n_m\Delta_{mw}$, separated by $2\chi_{q\text{-}m} + \Delta_{mw}$ and with a spectral weight closely related to p_{n_m}. (**B**) Measurement of the qubit spectrum for a coil current I = −5.02 mA as a function of the Kittel mode excitation frequency ω_{mw} and the spectroscopy frequency ω_s. The excitation frequency producing the maximum magnon-induced ac Stark shift of the qubit from ω_q (horizontal dashed line) yields an estimation of $\omega_m{}^g/2\pi \approx 7.95$ GHz (vertical dashed line). The Kittel mode spectrum, measured via its dispersive interaction with the probe mode, appears as a faint vertical line at ~7.95 GHz. The signature corresponding to the two-photon transition involving both the spectroscopy and the excitation photons and exciting both the qubit and a magnon (fig. S1) is indicated by the diagonal dashed line given by $\omega_s = \omega_q^{(n_m=0)} + 2\chi_{q\text{-}m} + \Delta_{mw}$, calculated with $\chi_{q\text{-}m}/2\pi$ = 1.5 MHz at $\omega_m{}^g/2\pi$ = 7.95 GHz.

coherent interaction between the qubit and the Kittel mode (*15*). The qubit-magnon coupling strength $g_{q\text{-}m}$ of 7.79 MHz, obtained from the magnon-vacuum Rabi splitting of the qubit (Fig. 1C), is much larger than both the power-broadened qubit linewidth $\gamma_q/2\pi$ = 1.74 MHz and the magnon linewidth $\gamma_m/2\pi$= 1.3 MHz.

We now investigate the dispersive regime of our hybrid system, where the detuning between the bare qubit and Kittel mode frequencies, $|\omega_q{}^{bare} - \omega_m{}^{bare}|$, is much larger than $g_{q\text{-}m}$. The exchange of quanta of excitations between the qubit and the Kittel mode, through virtual photons in the coupler cavity mode, is then highly

suppressed. The dispersive part of the qubit-magnon Hamiltonian is then given by

$$\hat{H}_{\text{q-m}}^{\text{disp}} = \hbar\chi_{\text{q-m}}\hat{\sigma}_z\hat{c}^\dagger\hat{c} \quad (1)$$

where $\hat{\sigma}_z = |e\rangle\langle e| - |g\rangle\langle g|$, with $|g(e)\rangle$ the ground (excited) state of the transmon qubit, $\hat{c}^\dagger$ ($\hat{c}$) is the magnon creation (annihilation) operator, and $\chi_{\text{q-m}}$ is the qubit-magnon dispersive shift (*4*, *16*). This dispersive interaction makes the qubit and magnon frequencies dependent on the state of the other system. More precisely, the qubit frequency $\omega_q^{(n_m)}$ depends on the magnon number state $|n_m = \{0, 1, 2, \ldots\}\rangle$, and the magnon frequency $\omega_m^{\,i}$ depends on the transmon state $|i = \{g, e, f, \ldots\}\rangle$. As illustrated in Fig. 2A, the strong dispersive regime, where $|2\chi_{\text{q-m}}| > \max[\gamma_q,\gamma_m]$, enables the observation of magnon number states $|n_m\rangle$ via magnon number–dependent ac Stark shift of the qubit frequency (*17*, *18*).

The qubit-magnon dispersive regime is investigated through spectroscopic measurements of the qubit while exciting the Kittel mode at frequency ω_{mw}, detuned by $\Delta_{mw} = \omega_m^{\,g} - \omega_{mw}$ from the dressed magnon frequency $\omega_m^{\,g}$. The measurement of the qubit spectrum while sweeping ω_{mw} for a coil current of −5.02 mA and a Kittel mode excitation power P_{mw} of 7.9 fW is shown in Fig. 2B. Near resonant excitation $\Delta_{mw} \sim 0$, the qubit is ac Stark–shifted by the magnon occupancy in the Kittel mode, a signature of the qubit-magnon dispersive interaction similar to the qubit-photon counterpart in circuit quantum electrodynamics experiments (*17*, *27*). The positive magnon-induced ac Stark shift shows that $\chi_{\text{q-m}} > 0$, and the excitation frequency producing the maximum shift indicates that $\omega_m^{\,g}/2\pi \approx 7.95$ GHz. Both these features are consistent with the hybrid system being in the straddling regime (fig. S1) (*21*, *28*). Notably, the signature corresponding to the two-photon transition, from $|g, n_m = 0\rangle$ to $|e, n_m = 1\rangle$, involving both the spectroscopy and the excitation photons and exciting both the qubit and a magnon (fig. S1), is also visible at $\omega_s = \omega_q^{(n_m=0)} + 2\chi_{\text{q-m}} + \Delta_{mw}$.

We now focus on resolving the magnon number states through measurements with the excitation frequency close to resonance with the Kittel mode ($\Delta_{mw} \ll \gamma_m$). In the qubit spectra shown in Fig. 3, the excitation frequency is fixed at 7.95 GHz, close to resonance with $\omega_m^{\,g}$ for $I = -5.02$ mA (Fig. 2B). The microwave excitation creates a magnon coherent state in the Kittel mode. When coherently driving the Kittel mode, we observe peaks in the qubit spectrum at frequencies higher than the zero-magnon peak. As shown next, these peaks correspond to different numbers of magnons in the Kittel mode.

To fit the data of Fig. 3, we used an analytical model of the spectrum of a qubit dispersively coupled to a harmonic oscillator (*17*). The asymmetric qubit line shape at $P_{mw} = 0$ is well reproduced by including in the fit the photonic contribution to the qubit line shape from the dispersive interaction between the qubit and the probe mode (section S4). The fitting parameters for each excitation power are the occupancy of the Kittel mode $\bar{n}_m^{\,g} = \langle \hat{n}_m \hat{\Pi}_q^g \rangle$ (where $\hat{\Pi}_q^g = |g\rangle\langle g|$ is the projector to the qubit ground state), the qubit-magnon dispersive shift ($\chi_{\text{q-m}}$), and the excitation detuning (Δ_{mw}) (Fig. 3A). More information on the theory and the fitting procedure can be found in sections S3 to S5. We find a detuning Δ_{mw} of −0.38 MHz, indicating a bare magnon frequency $\omega_m^{\,\text{bare}}$ of 7.9515 GHz. The condition for the dispersive regime is therefore respected with a detuning $|\omega_q^{\,\text{bare}} - \omega_m^{\,\text{bare}}|$ of 89 MHz, much larger than the qubit-magnon coupling strength. The qubit-magnon dispersive shift $\chi_{\text{q-m}}$ is found

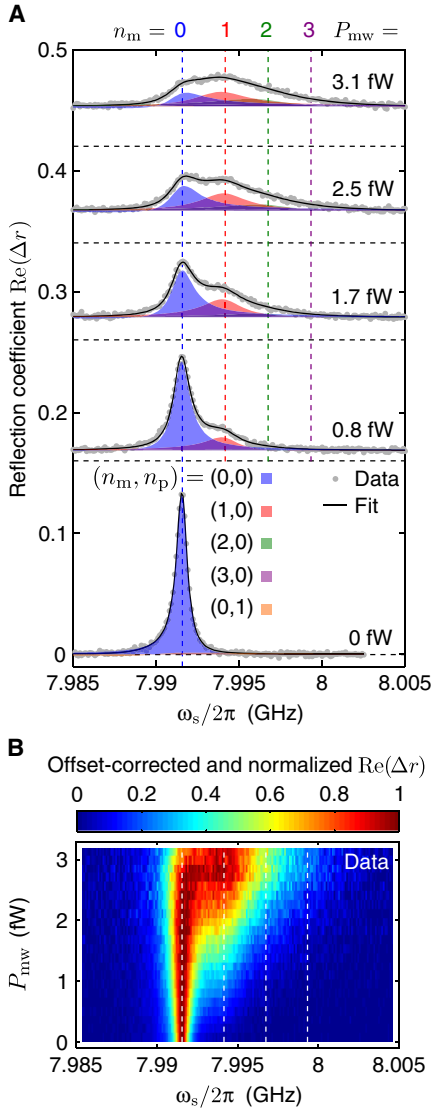

Fig. 3. Resolving magnon number states. (**A**) Measurements of the qubit spectrum at different Kittel mode excitation powers P_{mw} for a coil current of −5.02 mA and Kittel mode excitation frequency of 7.95 GHz. Black lines show fits of the data to the spectrum of a qubit dispersively coupled to a harmonic oscillator. Color-coded shaded areas show components of the spectrum corresponding to different photon number states $|n_p\rangle$ of the probe cavity mode and magnon number states $|n_m\rangle$. Vertical offsets are shown by horizontal dashed lines. (**B**) Measured qubit spectra as a function of P_{mw}. For clarity, after subtracting a power-dependent offset, Re(Δ*r*) is normalized relative to its maximum for each drive power. For both (A) and (B), vertical dashed lines indicate the frequencies of the qubit $|g\rangle \leftrightarrow |e\rangle$ transitions corresponding to the first four magnon number states, neglecting a power-dependent ac Stark shift, which is small relative to the dispersive shift per magnon for this range of P_{mw}.

to be 1.5 ± 0.1 MHz, in good agreement with the theoretical value of 1.27 MHz (fig. S1). Resolving magnon number states demonstrates that we have reached the strong dispersive regime of quantum magnonics, with the dispersive shift per magnon $2\chi_{\text{q-m}}$ being larger than both the power-broadened qubit linewidth $\gamma_q/2\pi = 0.78$ MHz and the magnon linewidth $\gamma_m/2\pi = 1.3$ MHz.

The average number of magnons $\bar{n}_m^{\,g}$ in the Kittel mode extracted from the fit of the data is shown in Fig. 4A. At the lowest excitation

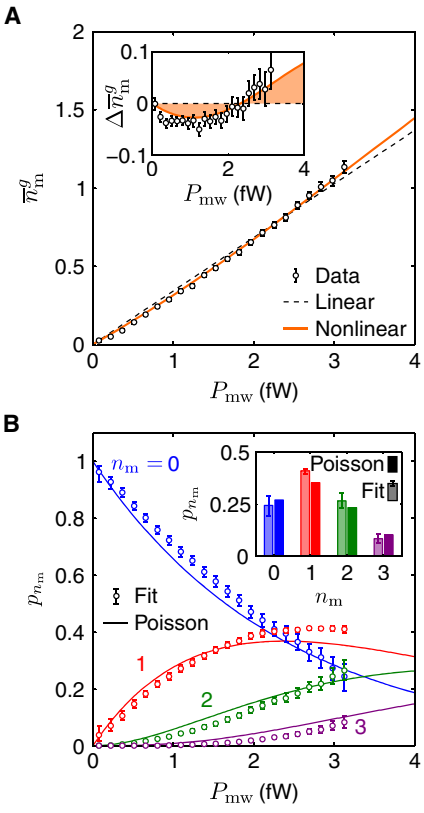

Fig. 4. Magnon occupancy and probability distribution. (**A**) Magnon occupancy $\bar{n}_m^g$ as a function of the excitation power P_{mw}. Dashed black line and solid orange line show fits to a driven linear and nonlinear Kittel mode, respectively. Inset: Deviations $\Delta\bar{n}_m^g$ from the linear fit, indicating a significant magnon Kerr nonlinearity. (**B**) Probability p_{n_m} of the first four magnon number states as a function of P_{mw}. Poisson distributions are shown as solid lines. Inset: p_{n_m} for P_{mw} = 3.1 fW. For both (A) and (B), error bars correspond to 95% confidence intervals.

power of 79 aW, we are able to resolve 0.026 ± 0.012 magnons in the Kittel mode of the ferromagnetic sphere containing about 1.4×10^{18} spins. We are therefore able to resolve a change in the magnetic moment of the ferromagnet equivalent to a single spin flipped among ~5×10^{19} spins. Within our resolution of about 0.01 magnons, no thermal occupancy of the Kittel mode is observed, indicating that the millimeter-sized ferromagnet is indeed in its magnon-vacuum state. Furthermore, the nonlinearity of $\bar{n}_m^g$ against the excitation power can be explained by a Kerr nonlinearity in the Kittel mode caused by the anharmonicity of the transmon (*3*, *29*). We find a Kerr coefficient of $-0.20\pm^{0.09}_{0.13}$ MHz in good agreement with the expected value of –0.12 MHz (fig. S1).

Finally, we estimate the probability p_{n_m} of having n_m magnons in the Kittel mode with

$$p_{n_m} \approx \int d\omega_s \, S_{n_m}(\omega_s)/S(\omega_s) \qquad (2)$$

where $S(\omega_s) \approx \Sigma_{n_m=0}^{10} S_{n_m}(\omega_s)$ is the qubit spectrum in the analytical model, to which data are fitted, and $S_{n_m}(\omega_s)$ is its component associated with the magnon number state $|n_m\rangle$. For $2\chi_{q\text{-}m} \gg \gamma_m$, the probability distribution calculated with Eq. 2 falls back to the Poisson distribution expected for a driven harmonic oscillator (section S5) (*17*). The probability distributions p_{n_m} of the first four magnon number states, shown in Fig. 4B, indicate small deviations from Poisson distributions. This is expected because the qubit-magnon dispersive shift is only slightly larger than the magnon linewidth in our hybrid system (section S5). Nevertheless, our ability to map the probability distribution of magnon number states to the spectrum of a qubit provides a novel tool for investigating quantum states in magnetostatic modes.

DISCUSSION

Looking forward, the strong dispersive interaction between magnons and a superconducting qubit demonstrated here should enable the encoding of the qubit into a superposition of magnon coherent states in a magnetostatic mode (*19*, *20*). However, to implement this encoding protocol, the qubit-magnon system needs to be deeper into the strong dispersive regime, either by increasing the qubit-magnon coupling strength or by decreasing the magnon linewidth in the quantum regime (*23*). Together with the recently demonstrated bidirectional conversion between microwave and optical photons in YIG (*12*), this could pave the way to the transfer of quantum states between superconducting qubits and photons in optical fibers. Combining two very promising candidates for both stationary and flying qubits, such a breakthrough would be an important step toward the realization of a superconducting qubit–based quantum network. Furthermore, the ability to count the number of magnons in a millimeter-sized ferromagnetic insulator in the quantum regime from zero up to a few magnons could be used to study microscopic mechanisms of collective spin excitations, such as decay, scattering, and coupling to a bath of two-level systems. Finally, the demonstrated architecture of quantum magnonics could also be used in applications in spintronics and spin-based quantum information processing (*30*).

MATERIALS AND METHODS

Figure S2 shows the instruments and components used in the experiment. Microwave powers P_r, P_s, and P_{mw} were calibrated using the input of the cavity as the reference point. At that reference point, the reflection coefficient r is in unity when $|\omega_r - \omega_{10p}| \gg \kappa_{10p}$, where ω_r is the readout frequency and ω_{10p} and κ_{10p} are the resonant frequency and the linewidth of the TE_{10p} cavity mode, respectively, with p = 1,2,3…. By taking into account the attenuation in cables outside and inside the dilution refrigerator, the total attenuations between the microwave sources and the input of the cavity are approximately 81, 122, and 121 dB for the readout, spectroscopy, and Kittel mode microwave excitations, respectively.

The yoke, coil, cavity, and YIG sphere of the hybrid system used in the paper were the same as in the study by Tabuchi *et al.* (*15*), whereas the transmon qubit was a different one. The oxygen-free copper microwave cavity had dimensions of 24 × 3 × 53 mm^3. An SMA (subminiature version A) connector connected to the cavity was used to measure the reflection coefficient r. A pair of disc-shaped neodymium permanent magnets, with a diameter of 10 mm and a thickness of 1 mm each, were placed at the ends of a magnetic yoke made of pure iron. The magnets produced a static field $B_0 \approx 0.29$ T in the 4-mm gap between them. The magnetic field can be additionally tuned by a current I in a 10^4-turn superconducting coil. The field-to-current conversion ratio is approximately 1.7 mT/mA. A YIG sphere glued to an aluminum oxide rod along the ⟨110⟩ crystal axis was mounted in the cavity at the center of the gap between the magnets.

The static field was applied in parallel with the ⟨100⟩ crystal axis. A transmon-type superconducting qubit, consisting of two large-area aluminum pads and a single Josephson junction ($Al/Al_2O_3/Al$), was fabricated on a silicon substrate and was mounted inside the cavity. The qubit and the YIG sphere were separated by 35 mm in the horizontal direction. A double-layer magnetic shield made of aluminum and pure iron covered half of the cavity to protect the qubit from the stray magnetic field of the magnet.

SUPPLEMENTARY MATERIALS

Supplementary material for this article is available at http://advances.sciencemag.org/cgi/content/full/3/7/e1603150/DC1

section S1. Hamiltonian of the hybrid system
section S2. Cavity-magnon coupling
section S3. Qubit spectrum in the dispersive regime
section S4. Qubit spectroscopy—Magnon vacuum state
section S5. Qubit spectroscopy—Magnon coherent state
section S6. Magnon Kerr nonlinearity
fig. S1. Qubit-magnon hybrid system.
fig. S2. Experimental setup.
fig. S3. Cavity-magnon coupling.
fig. S4. Power broadening of the qubit spectrum.
fig. S5. Dispersive qubit-magnon interaction.
fig. S6. Probability distributions.
fig. S7. Magnon Kerr nonlinearity.
fig. S8. Effect of the finite Kerr nonlinearity on the magnon probability distribution.
table S1. Parameters of the hybrid system.
table S2. Comparison between experimental and theoretical values.
table S3. Linewidths of the hybrid system.
table S4. Experimental parameters of the measurements.
References (*31*–*34*)

REFERENCES AND NOTES

1. S. Haroche, J.-M. Raimond, *Exploring the Quantum* (Oxford Univ. Press, 2006).
2. M. Hofheinz, H. Wang, M. Ansmann, R. C. Bialczak, E. Lucero, M. Neeley, A. D. O'Connell, D. Sank, J. Wenner, J. M. Martinis, A. N. Cleland, Synthesizing arbitrary quantum states in a superconducting resonator. *Nature* **459**, 546–549 (2009).
3. G. Kirchmair, B. Vlastakis, Z. Leghtas, S. E. Nigg, H. Paik, E. Ginossar, M. Mirrahimi, L. Frunzio, S. M. Girvin, R. J. Schoelkopf, Observation of quantum state collapse and revival due to the single-photon Kerr effect. *Nature* **495**, 205–209 (2013).
4. A. Blais, R.-S. Huang, A. Wallraff, S. M. Girvin, R. J. Schoelkopf, Cavity quantum electrodynamics for superconducting electrical circuits: An architecture for quantum computation. *Phys. Rev. A* **69**, 062320 (2004).
5. A. Wallraff, D. I. Schuster, A. Blais, L. Frunzio, R.-S. Huang, J. Majer, S. Kumar, S. M. Girvin, R. J. Schoelkopf, Strong coupling of a single photon to a superconducting qubit using circuit quantum electrodynamics. *Nature* **431**, 162–167 (2004).
6. T. D. Ladd, F. Jelezko, R. Laflamme, Y. Nakamura, C. Monroe, J. L. O'Brien, Quantum computers. *Nature* **464**, 45–53 (2010).
7. J. Kelly, R. Barends, A. G. Fowler, A. Megrant, E. Jeffrey, T. C. White, D. Sank, J. Y. Mutus, B. Campbell, Y. Chen, Z. Chen, B. Chiaro, A. Dunsworth, I.-C. Hoi, C. Neill, P. J. J. O'Malley, C. Quintana, P. Roushan, A. Vainsencher, J. Wenner, A. N. Cleland, J. M. Martinis, State preservation by repetitive error detection in a superconducting quantum circuit. *Nature* **519**, 66–69 (2015).
8. M. Aspelmeyer, T. J. Kippenberg, F. Marquardt, Cavity optomechanics. *Rev. Mod. Phys.* **86**, 1391–1452 (2014).
9. J. Bochmann, A. Vainsencher, D. D. Awschalom, A. N. Cleland, Nanomechanical coupling between microwave and optical photons. *Nat. Phys.* **9**, 712–716 (2013).
10. R. W. Andrews, R. W. Peterson, T. P. Purdy, K. Cicak, R. W. Simmonds, C. A. Regal, K. W. Lehnert, Bidirectional and efficient conversion between microwave and optical light. *Nat. Phys.* **10**, 321–326 (2014
11. A. Osada, R. Hisatomi, A. Noguchi, Y. Tabuchi, R. Yamazaki, K. Usami, M. Sadgrove, R. Yalla, M. Nomura, Y. Nakamura, Cavity optomagnonics with spin-orbit coupled photons. *Phys. Rev. Lett.* **116**, 223601 (2016).
12. R. Hisatomi, A. Osada, Y. Tabuchi, T. Ishikawa, A. Noguchi, R. Yamazaki, K. Usami, Y. Nakamura, Bidirectional conversion between microwave and light via ferromagnetic magnons. *Phys. Rev. B* **93**, 174427 (2016).
13. X. Zhang, N. Zhu, C.-L. Zou, H. X. Tang, Optomagnonic whispering gallery microresonators. *Phys. Rev. Lett.* **117**, 123605 (2016).
14. J. A. Haigh, A. Nunnenkamp, A. J. Ramsay, A. J. Ferguson, Triple-resonant Brillouin light scattering in magneto-optical cavities. *Phys. Rev. Lett.* **117**, 133602 (2016).
15. Y. Tabuchi, S. Ishino, A. Noguchi, T. Ishikawa, R. Yamazaki, K. Usami, Y. Nakamura, Coherent coupling between a ferromagnetic magnon and a superconducting qubit. *Science* **349**, 405–408 (2015).
16. Y. Tabuchi, S. Ishino, A. Noguchi, T. Ishikawa, R. Yamazaki, K. Usami, Y. Nakamura, Quantum magnonics: The magnon meets the superconducting qubit. *C. R. Phys.* **17**, 729–739 (2016).
17. J. Gambetta, A. Blais, D. I. Schuster, A. Wallraff, L. Frunzio, J. Majer, M. H. Devoret, S. M. Girvin, R. J. Schoelkopf, Qubit-photon interactions in a cavity: Measurement-induced dephasing and number splitting. *Phys. Rev. A* **74**, 042318 (2006).
18. D. I. Schuster, A. A. Houck, J. A. Schreier, A. Wallraff, J. M. Gambetta, A. Blais, L. Frunzio, J. Majer, B. Johnson, M. H. Devoret, S. M. Girvin, R. J. Schoelkopf, Resolving photon number states in a superconducting circuit. *Nature* **445**, 515–518 (2007).
19. Z. Leghtas, G. Kirchmair, B. Vlastakis, M. H. Devoret, R. J. Schoelkopf, M. Mirrahimi, Deterministic protocol for mapping a qubit to coherent state superpositions in a cavity. *Phys. Rev. A* **87**, 042315 (2013).
20. B. Vlastakis, G. Kirchmair, Z. Leghtas, S. E. Nigg, L. Frunzio, S. M. Girvin, M. Mirrahimi, M. H. Devoret, R. J. Schoelkopf, Deterministically encoding quantum information using 100-photon Schrödinger cat states. *Science* **342**, 607–610 (2013).
21. J. Koch, T. M. Yu, J. Gambetta, A. A. Houck, D. I. Schuster, J. Majer, A. Blais, M. H. Devoret, S. M. Girvin, R. J. Schoelkopf, Charge-insensitive qubit design derived from the Cooper pair box. *Phys. Rev. A* **76**, 042319 (2007).
22. H. Huebl, C. W. Zollitsch, J. Lotze, F. Hocke, M. Greifenstein, A. Marx, R. Gross, S. T. B. Goennenwein, High cooperativity in coupled microwave resonator ferrimagnetic insulator hybrids. *Phys. Rev. Lett.* **111**, 127003 (2013).
23. Y. Tabuchi, S. Ishino, T. Ishikawa, R. Yamazaki, K. Usami, Y. Nakamura, Hybridizing ferromagnetic magnons and microwave photons in the quantum limit. *Phys. Rev. Lett.* **113**, 083603 (2014).
24. M. Goryachev, W. G. Farr, D. L. Creedon, Y. Fan, M. Kostylev, M. E. Tobar, High-cooperativity cavity QED with magnons at microwave frequencies. *Phys. Rev. Appl.* **2**, 054002 (2014).
25. X. Zhang, C.-L. Zou, N. Zhu, F. Marquardt, L. Jiang, H. X. Tang, Magnon dark modes and gradient memory. *Nat. Commun.* **6**, 8914 (2015).
26. N. J. Lambert, J. A. Haigh, S. Langenfeld, A. C. Doherty, A. J. Ferguson, Cavity-mediated coherent coupling of magnetic moments. *Phys. Rev. A* **93**, 021803(R) (2016).
27. D. I. Schuster, A. Wallraff, A. Blais, L. Frunzio, R.-S. Huang, J. Majer, S. M. Girvin, R. J. Schoelkopf, ac Stark shift and dephasing of a superconducting qubit strongly coupled to a cavity field. *Phys. Rev. Lett.* **94**, 123602 (2005).
28. K. Inomata, T. Yamamoto, P.-M. Billangeon, Y. Nakamura, J. S. Tsai, Large dispersive shift of cavity resonance induced by a superconducting flux qubit in the straddling regime. *Phys. Rev. B* **86**, 140508(R) (2012).
29. J. Bourassa, F. Beaudoin, J. M. Gambetta, A. Blais, Josephson-junction-embedded transmission-line resonators: From Kerr medium to in-line transmon. *Phys. Rev. A* **86**, 013814 (2012).
30. P. Andrich, C. F. de las Casas, X. Liu, H. L. Bretscher, J. R. Berman, F. J. Heremans, P. F. Nealey, D. D. Awschalom, Hybrid nanodiamond-YIG systems for efficient quantum information processing and nanoscale sensing. arXiv:1701.07401 (2017).
31. M. D. Reed, L. DiCarlo, B. R. Johnson, L. Sun, D. I. Schuster, L. Frunzio, R. J. Schoelkopf, High-fidelity readout in circuit quantum electrodynamics using the Jaynes-Cummings nonlinearity. *Phys. Rev. Lett.* **105**, 173601 (2010).
32. J. A. Haigh, N. J. Lambert, A. C. Doherty, A. J. Ferguson, Dispersive readout of ferromagnetic resonance for strongly coupled magnons and microwave photons. *Phys. Rev. B* **91**, 104410 (2015).
33. J. R. Johansson, P. D. Nation, F. Nori, QuTiP: An open-source Python framework for the dynamics of open quantum systems. *Comput. Phys. Commun.* **183**, 1760–1772 (2012).
34. J. R. Johansson, P. D. Nation, F. Nori, QuTiP 2: A Python framework for the dynamics of open quantum systems. *Comput. Phys. Commun.* **184**, 1234–1240 (2013).

Acknowledgments: We acknowledge K. Usami, A. Blais, J. Bourassa, and M. Pioro-Ladrière for useful discussions and P.-M. Billangeon for fabricating the transmon qubit. **Funding:** This work was partly supported by the Project for Developing Innovation System of MEXT (Ministry of Education, Culture, Sports, Science and Technology), JSPS (Japan Society for the Promotion of Science) KAKENHI (Grants-in-Aid for Scientific Research) (grant nos. 26600071 and 26220601), NICT (National Institute of Information and Communications Technology), JST (Japan Science and Technology Agency) ERATO (Exploratory Research for Advanced Technology) (grant no. JPMJER1601), the Murata Science Foundation, the Research Foundation for Opto-Science and Technology, the Tateisi Science and Technology Foundation, the JSPS

Summer Program, and the Natural Sciences and Engineering Research Council of Canada.
Author contributions: The measurements were carried out by D.L.-Q. and S.I., with input from all authors. D.L.-Q., Y.T., and Y.N. analyzed the data and wrote the manuscript with input from all authors. Y.T., S.I., and Y.N. conceived the hybrid system with input from A.N., T.I., and R.Y. **Competing interests:** The authors declare that they have no competing interests. **Data and materials availability:** All data needed to evaluate the conclusions in the paper are present in the paper and/or the Supplementary Materials. Additional data related to this paper may be requested from the authors.

Submitted 12 December 2016
Accepted 18 May 2017
Published 5 July 2017
10.1126/sciadv.1603150

Citation: D. Lachance-Quirion, Y. Tabuchi, S. Ishino, A. Noguchi, T. Ishikawa, R. Yamazaki, Y. Nakamura, Resolving quanta of collective spin excitations in a millimeter-sized ferromagnet. *Sci. Adv.* **3**, e1603150 (2017).